TISSUE ENGINEERING: Part A
Volume 15, Number 2, 2009

DOI: 10.1089/ten.tea.2007.0371

Original Papers

Biomineralization of a Self-Assembled Extracellular Matrix for Bone Tissue Engineering

Yizhi Meng, Ph.D.,[1] Yi-Xian Qin, Ph.D.,[1] Elaine DiMasi, Ph.D.,[2] Xiaolan Ba, M.S.,[3] Miriam Rafailovich, Ph.D.,[3] and Nadine Pernodet, Ph.D.[3]

Understanding how biomineralization occurs in the extracellular matrix (ECM) of bone cells is crucial to the understanding of bone formation and the development of a successfully engineered bone tissue scaffold. It is still unclear how ECM mechanical properties affect protein–mineral interactions in early stages of bone mineralization. We investigated the longitudinal mineralization properties of MC3T3-E1 cells and the elastic modulus of their ECM using shear modulation force microscopy, synchrotron grazing incidence X-ray diffraction (GIXD), scanning electron microscopy, energy dispersive X-ray spectroscopy, and confocal laser scanning microscopy (CLSM). The elastic modulus of the ECM fibers underwent significant changes for the mineralizing cells, which were not observed in the nonmineralizing cells. On substrates conducive to ECM network production, the elastic modulus of mineralizing cells increased at time points corresponding to mineral production, whereas that of the nonmineralizing cells did not vary over time. The presence of hydroxyapatite in mineralizing cells and the absence thereof in the nonmineralizing ones were confirmed by GIXD, and CLSM showed that a restructuring of actin occurred only for mineral-producing cells. These results show that the correct and complete development of the ECM network is required for osteoblasts to mineralize. This in turn requires a suitably prepared synthetic substrate for bone development to succeed *in vitro*.

Introduction

Successful bone tissue engineering requires that bone cells, extracellular matrix (ECM), and scaffold material be addressed holistically as a three-component system. Up to now, cell–ECM and cell–scaffold interactions have been only partially understood, while ECM–scaffold interactions have barely begun. In this paper we will demonstrate how the three-component system of osteoblasts, ECM, and growth substrate can be probed by *in situ* imaging and mechanical modulus measurements, at very early stages of biomineralization. The bone ECM is a rich, dynamic reservoir for structural proteins, matrix-degrading proteases, and growth factors.[1] The underlying structure and function of ECM proteins and how they contribute to cell-mediated mineralization are yet to be thoroughly explored. Earlier works by developmental biologists demonstrated that cell–ECM interactions can direct tissue-specific function.[2] Marsh *et al.*[3] later established that a properly matured collagenous matrix can alone support mineral grown in the absence of osteoblasts. More recently Chen *et al.*[4] demonstrated that a purified, cell-free ECM is able to promote bone marrow mesenchymal stem cell growth and proliferation better than coatings of a single ECM protein. A major strategy in designing biomimetic materials is to adsorb the ECM proteins so that they can mediate tissue formation through their interactions with the cells.[5] The difficulty of studying the ECM arises from the length hierarchical organization of its components, which range from below 100 nm (such as tropocollagen) to 20 μm in size (such as cells). In the last decade, advances in genomics and proteomics have made it possible to better understand the ECM at the molecular and cellular levels. This in turn has led to the examination of cell and ECM biomechanics at these fundamentally small length scales. One technique that has been developed for this very purpose is shear modulation force microscopy (SMFM), an atomic force microscope–based technique that probes the mechanical properties at the nanoscale.[6,7] Relatively few studies have thus far elucidated the ability of an ECM to guide the fate of osteogenic cells,[8] particularly with respect to the effects of its mechanical properties during cell-mediated mineralization. It may require longitudinal characterization

[1]Department of Biomedical Engineering, Stony Brook University, Stony Brook, New York.
[2]National Synchrotron Light Source, Brookhaven National Laboratory, Upton, New York.
[3]Department of Materials Science and Engineering, Stony Brook University, Stony Brook, New York.

of ECM development along with interactive cellular biomechanical properties, which to our knowledge has not been done. The advantage of the SMFM is that we can image and measure the mechanical properties of cells and ECM simultaneously *in vitro*. This is not possible to do with other methods such as scanning electron microscopy (SEM),[9] and in our work we present findings from both of these techniques. It is important to measure cells and ECM simultaneously, and a full understanding of the functional role of a cell-generated ECM has the potential for developing artificial ECM toward applications in tissue engineering. We therefore use this new technique to introduce the roles of ECM, substrate, and cells as an integral system of bone mineralization.

Investigating the development of bone matrix mineralization is of fundamental interest to bone tissue engineers.[10] The mineral phase of bone is a poorly crystalline, carbonate-rich analog of the hydroxyapatite (HAP) mineral that exists in nature.[11] Histological methods of testing for the formation of bone mineral in osteoblasts are often difficult to quantify and may introduce false positives.[12] Spectroscopic studies of both primary cells[13] and the MC3T3-E1 cell line[14] have shown that osteoblasts in culture produce a poorly carbonated apatitic mineral similar to bone tissue. However, the study of the mineral phase is complicated by the presence of organic matrix components, which reduce the resolution of spectral analyses.[15] A possible rapid transition of initial nonapatitic calcium phosphate to crystalline apatite may occur, but is likely to escape detection.[15] Crystallographic studies of bioapatites are often derived from powder diffraction of synthetic samples,[16–18] which greatly differ from biological apatites in chemical and physical properties. For these reasons, the fundamental question of how biological HAP is first deposited in the ECM and initiates mineralization remains to be answered.

Meanwhile, medical applications demand biocompatible materials for regenerative tissue engineering and the treatment of bone fractures.[5,19–22] The diversity of available polymers offers extensive freedom in designing the structure and composition of scaffolds, and polymeric materials are a logical choice for tissue engineering purposes.[23] Although natural polymers may promote cell adhesion and growth, their mechanical properties and biodegradability are not as easily controlled as those of synthetic polymers.[23] Thus, synthetic, biodegradable polymers have emerged as potential scaffolding substrates.[24,25] An ideal combination of scaffold, cells, and bioactive molecules has yet to be created for bone tissue engineering.[10]

It has been well known that fibronectin is an essential protein in the cell ECM. Adsorbed fibronectin has been found to enhance osteogenic differentiation,[26–29] increase adhesion strength of human leukemia cells,[30] induce cell spreading and the formation of stress fibers in corneal fibroblasts,[31] and is a crucial component in wound healing.[32] Undoubtedly, a successfully engineered scaffold would need to provide an optimal substrate for fibronectin. Recently, it was demonstrated[33] that fibronectin can be induced to self-assemble into a fibrillar network on a densely charged surface, such as sulfonated polystyrene (SPS) (Supplemental Fig. 1, available online at www.liebertonline.com/ten). This is in direct contrast with tissue culture–grade polystyrene, on which fibronectin remains in a globular, insoluble form that does not fibrillize.[33] Calcification has also been shown to occur preferentially on networked ECM protein fibers, and not on unstructured protein.[7] These *in vitro* discoveries regarding the interrelation between protein and SPS are vital clues to the understanding of biomineralization and stress the importance of protein–mineral and cell–mineral interactions during the early stages of *in vivo* crystallization. A full understanding of cell–mineral phenomena in culture or *in vivo*, therefore, requires as full a characterization as possible of individual ECM components and the ECM as a whole. There is abundant information in the literature on ECM, bone mineralization, and tissue scaffolds, but in the form of separately studied entities. Never before has there been a unified analysis that considers the close interrelation of all three. We here demonstrate that by disrupting any one of this triad—a properly formed ECM, the osteogenic ability of the cell, or a suitable scaffold—bone mineralization cannot occur.

Thus, the objective of this study is to develop a novel, interdisciplinary approach to characterize the longitudinal mineralization process of osteoblasts and their ECM on two substrates, bare silicon (Si) and Si coated with SPS. We hypothesize that SPS is directly implicated in the ECM development and mineral production of both mineralizing and nonmineralizing osteoblasts and that mechanical differences in ECM components affect the overall osteogenic capability.

Experimental Procedure

Cell culture

Two subclones of MC3T3-E1 cells (mineralizing and nonmineralizing) were maintained at 37°C (5% CO_2, humidified) in α-MEM culture medium supplemented with 10% fetal bovine serum (FBS) (Invitrogen, Carlsbad, CA), 100 units/mL penicillin and 100 μg/mL streptomycin (Invitrogen), 50 μg/mL L-ascorbic acid (Sigma, St. Louis, MO), and 4 mM β-glycerophosphate (Sigma). Fresh medium was given every 2 or 3 days. Cells were seeded at an initial density of 50,000 cells per cm^2 in 24-well tissue culture plates (BD Biosciences, Franklin Lakes, NJ). For ECM visualization, cells were seeded at a lower density (2000 cells per cm^2). The MC3T3-E1 cell line forms a bone-like mineralized ECM and is a good model system for studying osteogenic development.[34] The nonmineralizing cells were used to investigate whether or not they produce the same ECM as the mineralizing cells, and whether the ECM in this particular subclone is responsible for the lack of biomineralization.

Substrate preparation

Si substrates were spincoated with 20-nm-thick SPS films as previously described.[7] Those substrates that were not coated with SPS were autoclaved prior to cell culture.

Atomic force microscopy and SMFM

Atomic force microscopy (AFM) measurements were done in conjunction with SMFM at room temperature on ECM fibers and living cells immersed in CO_2-independent medium (Invitrogen) supplemented with 10% FBS, 100 units/mL penicillin, and 100 μg/mL streptomycin. Mechanical modulus of the fibers and the cells was measured using a Digital Instruments 3000 atomic force microscope (Santa Barbara, CA) in contact mode with a silicon nitride tip

(Thermal Microscopes, spring constant 0.06 N/m) (Supplemental Fig. 2, available online at www.liebertonline.com/ten). The x-direction piezo was oscillated at a sinusoidal frequency of 1400 Hz, and a constant normal force of 25 nN was applied to maintain contact between the tip and the cell surface. Because the amplitude response of the tip is a function of the normal force and the physical properties of the sample in which the tip is partially buried, the ratio of the response amplitude to the driving force can be used to derive the Young's modulus, E[6] (Supplemental Fig. 3, available online at www.liebertonline.com/ten). At least five fibers were measured from each sample. Each cell was measured at three locations: one at the center and two at a 500-nm offset from the center. Three measurements were done at each location, totaling nine measurements for each cell. Three different cells from each sample were examined.

SEM and energy dispersive X-ray spectroscopy

At days 14, 21, and 28, cells cultured on SPS were rinsed with phosphate-buffered saline (PBS) and deionized water, fixed with 70% ethyl alcohol and air dried, and imaged in a scanning electron microscope (JEOL JSM 6400, 20 keV accelerating voltage) at the Center for Functional Nanomaterials, Brookhaven National Laboratory. Energy dispersive X-ray spectroscopy (EDS) was used to calculate the Ca/P ratio in the ECM fibers and particles. Data from three fibers and three calcium particulates were taken from each sample. A commercial synthetic sample of HAP (Product #574791; Sigma) was also evaluated using EDS. We found that the usual carbon coating of samples in preparation for EDS measurement was not necessary in our case, as the calcified matrix provided excellent contrast.

Grazing incidence X-ray diffraction

Synchrotron grazing incidence X-ray diffraction (GIXD) experiments were carried out on beamline X6B at the National Synchrotron Light Source at Brookhaven National Laboratory. MC3T3-E1 cells cultured for 1, 7, 14, 21, and 28 days on SPS were investigated using focused X-ray beam at 0.6525 Å wavelength (spot size: 0.25-mm high, and 0.4-mm wide). In addition, the commercial synthetic HAP (Product #574791; Sigma) was examined in GIXD geometry as a powder dusted on a blank SPS substrate and in transmission in a glass capillary tube (1.0-mm diameter) (Supplemental Fig. 4, available online at www.liebertonline.com/ten). Samples were mounted in air 150 mm from the detector screen. Grazing incidence diffraction patterns with incident angle 0–2° were recorded using an X-ray CCD detector (MAR, Rayonix LLC, Evanston, IL, or Princeton Instruments, Trenton, NJ) and calibrated using a standard Al_2O_3 powder plate.

Data analysis

Crystallite size was measured according to the Scherrer method[35,36]:

$$L = \frac{K\lambda}{B_m \cos\theta_B} \quad (1)$$

where L is the volume-weighted average crystallite size, K is a unit cell geometry–dependent constant approximated to unity, λ is the wavelength of the X-ray, B_m is the full-width-half-maximum of the peak of interest, and θ_B is the Bragg angle.

Confocal laser scanning microscopy

MC3T3-E1 cells cultured for 1, 7, 14, 21, and 28 days were rinsed with PBS, fixed with 3.7% formaldehyde (in PBS), and stained with 30 μg/mL propidium iodide (in PBS) for nuclei visualization. A 3% solution of Alexa Fluor 488 Phalloidin (Invitrogen) in PBS was added to the cells for F-actin visualization. Cells immersed in PBS were imaged using a Leica Confocal Laser Scanning Microscope with a 63× water objective lens. The average volume of the nuclei in each sample was calculated based on the cross-sectional height measured from Z-scans and the equatorial radii measured from the two-dimensional images.

Results

Formation of the ECM

SPS-coated Si that was incubated in PBS only (Fig. 1A) was used as a control and has a height variation less than 500 nm, showing no other morphological features after 1 day. SPS that was incubated for 1 day in serum-containing tissue culture medium (Fig. 1B) shows that small amounts of protein globules of height ~500 nm can be imaged on the surface. When cells are cultured on the SPS substrate, fibrillar networks appear due to cellular deposition of ECM proteins (Fig. 1C–H, K). For all MC3T3-E1 cells cultured on SPS, there clearly was a fibrillar network in the intercellular regions by day 1 (Fig. 1C, D). By day 7, greater connectivity was seen among these fibers (Fig. 1E, F) and on day 14, the fibers appeared larger in width (Fig. 1G, H). On the contrary, no fibers were seen on Si for either subclone (Fig. 1I, J, and unpublished data). An image of a 7-day mineralizing MC3T3-E1 cell is shown additionally to illustrate the distribution of the ECM network relative to the cell (Fig. 1K).

For both subclones, the ECM fibers increased in height with time (Fig. 2), with a slightly broader distribution seen in the nonmineralizing culture. The average heights of these fibers were 1 and 1.6 μm on days 1 and 7, respectively, for both subclones. On day 14 the average fiber height was 2.3 μm for the mineralizing and 2.7 μm for the nonmineralizing culture, in much broader distributions ranging from less than 1 to greater than 4 μm. From these results it is clear that the ECM fibers in both cultures develop at about the same rate regardless of the subclone. On days 21 and 28, the ECM fibers were occluded by the cells (data not shown).

SMFM measurements of the ECM fibers (Fig. 3) showed that on day 1 the fibers in the nonmineralizing culture had stiffnesses, which approximately doubled by day 7. Fibers in the mineralizing ECM were dramatically different. On day 1 they were more than 10 times as stiff as the nonmineralizing culture. However, they evolved by day 7 into two distinct moieties, as shown by a bipolar distribution of SMFM response curve slopes (inset Fig. 3), with much lower moduli. Half of the mineralizing ECM fibers were almost twice as stiff as the nonmineralizing fibers, while the other half were softer. These results imply that considerable evolution of the ECM takes place in osteoblasts during this interval, which is unachievable for the nonmineralizing subclone. By day 14, no significant difference was found between the elastic

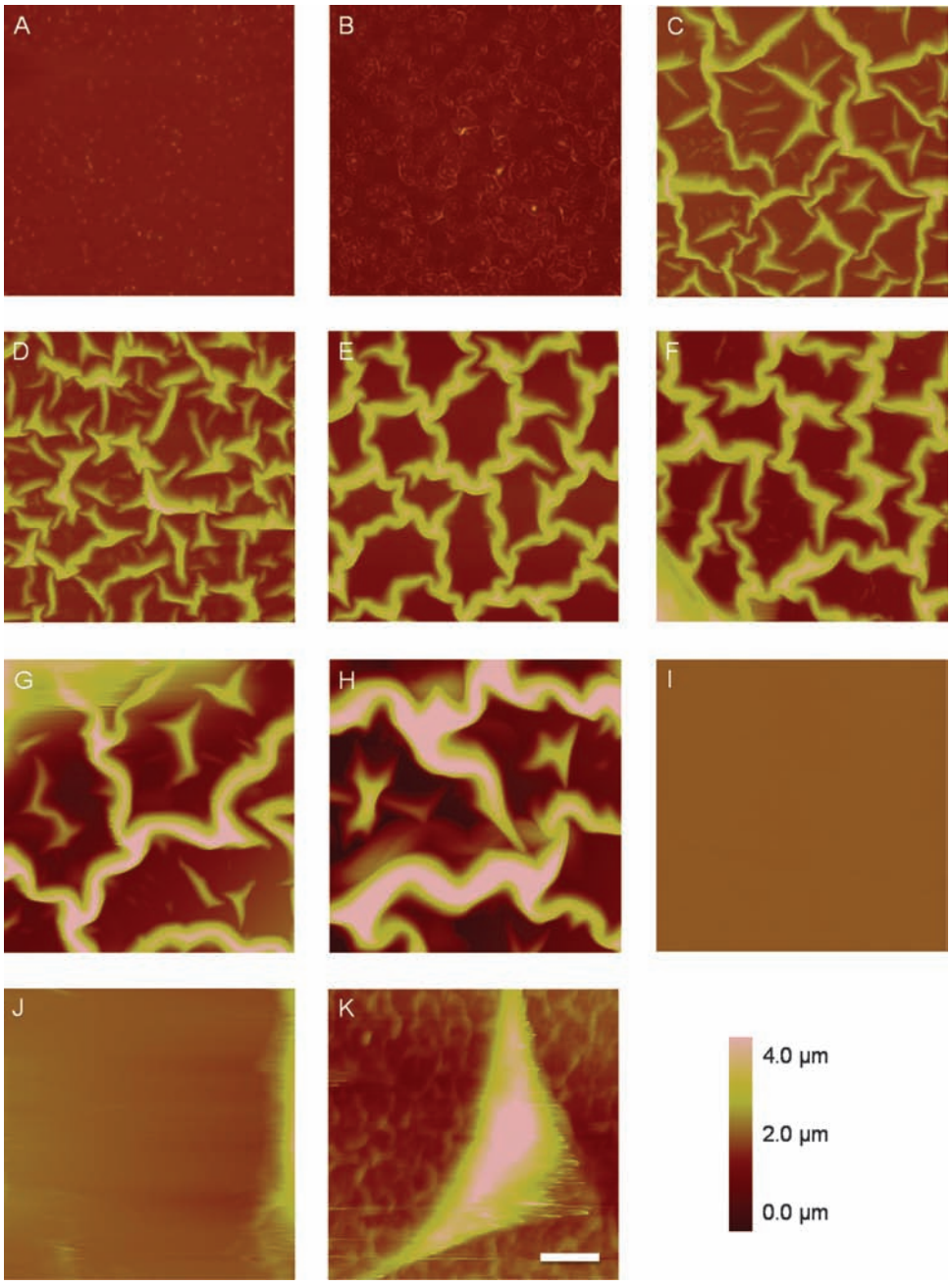

FIG. 1. Atomic force height micrographs of (**A**) blank SPS-coated Si after 1 day of incubation in PBS, (**B**) blank SPS-coated Si after 1 day of incubation in tissue culture medium supplemented with serum, and of intercellular regions on SPS containing 1-, 7-, and 14-day-old mineralizing (**C, E, G**) and nonmineralizing (**D, F, H**) MC3T3-E1 cells. ECM fibers are not present in regions near 7-day-old mineralizing (**I**) or nonmineralizing (**J**) MC3T3-E1 cells cultured on bare Si alone. An AFM of ECM fibers surrounding a 7-day-old mineralizing MC3T3-E1 cell on SPS is shown in (**K**) as an example of the intercellular regions. Bar = 10 μm. Color images available online at www.liebertonline.com/ten.

moduli of the fibers in either culture, but the mineralizing culture maintained a bimodal distribution of moduli (data not shown). It has already been shown by Franceschi and Iyer[37] that when ascorbic acid and β-glycerophosphate are added to the medium, MC3T3-E1 cells begin to accumulate collagen as early as 1 day later. It is very likely that the two subclones used in our study were synthesizing collagen (and most probably other ECM proteins) at different rates, which might explain the extremely high elastic modulus in the mineralizing ECM relative to the nonmineralizing ECM on day 1. We also know from another study by Wang *et al.*[38] that both mineralizing and nonmineralizing subclones of MC3T3-E1 produce comparable amounts of collagen and express similar levels of osteoblast-specific factor 2 mRNA, which is needed for osteoblast formation. Wang's group also showed that nonmineralizing MC3T3-E1 do not make a significant amount of osteocalcin, bone sialoprotein, or alkaline phosphatase. We must keep in mind that the types of ECM proteins in our study were not identified, and that matrix components other than collagen are very likely to be

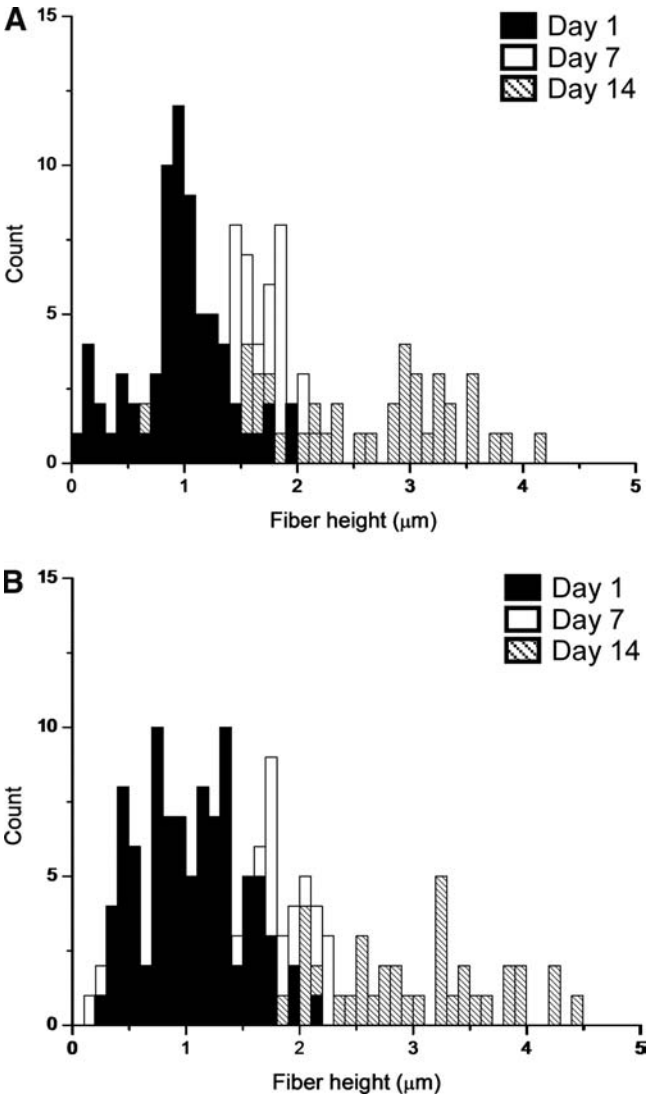

FIG. 2. Histograms of ECM fiber height from regions shown in Figure 1. The average fiber height of the mineralizing subclone (**A**) was 1 (day 1), 1.6 (day 7), and 2.3 μm (day 14). The average fiber height of the nonmineralizing subclone (**B**) was 1 (day 1), 1.6 (day 7), and 2.7 μm (day 14). On days 21 and 28, the ECM fibers were occluded by the cells (data not shown).

present in these networks. The strength of our study is that we have direct access to ECM mechanical measurements, which show unequivocally that there is a difference between the two subclones we tested, even if they were derived from the same parent cell line. What we find particularly intriguing is the difference in stiffness of the day-1 ECM fibers. It has been shown by Lo *et al.*[39] that fibroblast migration is enhanced on a more rigid surface, and in other analogous studies, muscle cells[40,41] exhibited preferential alignment and spreading on stiffer substrates. Our data suggest that the stiffer ECM fibers produced by the mineralizing subclone within the first day may have enhanced osteoblast cell migration, differentiation, and mineral formation.

SMFM measurements could be performed on living MC3T3-E1 cells themselves, on both SPS and Si. The elastic modulus of the mineralizing subclone cultured on SPS

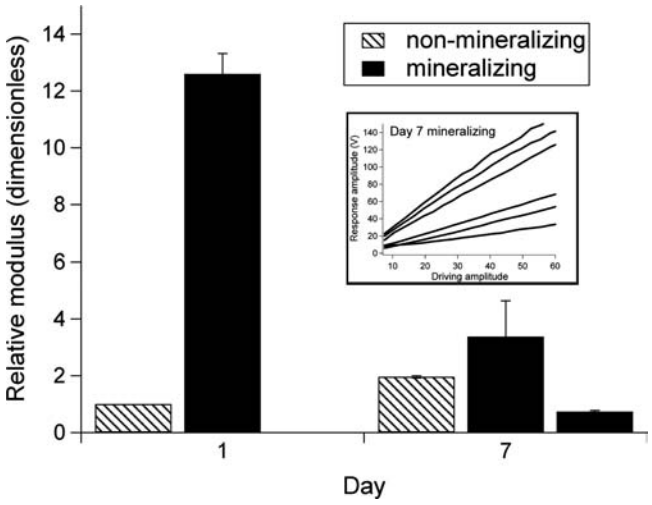

FIG. 3. Mean values (±SE) of the relative elastic modulus of the ECM fibers in the intercellular regions of MC3T3-E1. Modulus values were normalized relative to the day 1 value of nonmineralizing ECM. (Inset: raw SMFM response curves for mineralizing ECM on day 7. On the basis of the two clusters of slopes yielding distinctly different modulus values, we represent their relative modulus as a bimodal distribution, with two bars in the histogram.) Measurements were done with an atomic force microscope in contact mode with a silicon nitride tip (spring constant 0.06 N/m).

(Fig. 4A, —●—) increased linearly during the first 3 weeks, and did not change significantly from day 21 to day 28. In contrast, the same subclone on Si (Fig. 4B, —▲—) did not show any significant change in elastic modulus with time. The nonmineralizing cells did not increase in elastic modulus on either SPS (Fig. 4A, —○—) or Si (Fig. 4B, —△—). Significant changes in cell mechanics only occur for mineralizing cells grown on a substrate conducive to ECM formation.

Mineralization of the ECM

SEM of mineralizing MC3T3-E1 after 1, 7, 14, 21, and 28 days of differentiation (Fig. 5A, C, E, G, and I) showed fibrillar networks of ECM proteins similar to those seen in AFM experiments (Fig. 1). The meshing in these networks became progressively finer with time, and dispersed among them were calcium-containing particles as large as 10 μm in diameter. In addition, many of the 28-day particles were found at the intersections of ECM fibers (Fig. 5G, I), very much like calcite particles observed in the *in vitro* elastin mineralization experiment of Subburaman *et al.*[7] In contrast to the mineralizing osteoblasts, the ECM of the nonmineralizing cells appeared dark in the SEM (Fig. 5B, D, F, H, and I), and EDS showed that the particles found on them did not contain calcium.

EDS measurements of the Ca/P ratios of mineralizing cells on SPS were zero for days 1 and 7, and similar for the fibers and the particulates from day 14 (0.6) and day 28 (1.1–1.2) (Fig. 6). Interestingly, particles found in the 21-day mineralizing culture contained much more calcium (Ca/P = 1.0) compared to their surrounding ECM fibers (Ca/P = 0.3). At this time we do not know whether this was a result from the loss of calcium or an increase in phosphorus in the fibers between days 14 and 21. The Ca/P ratio of the

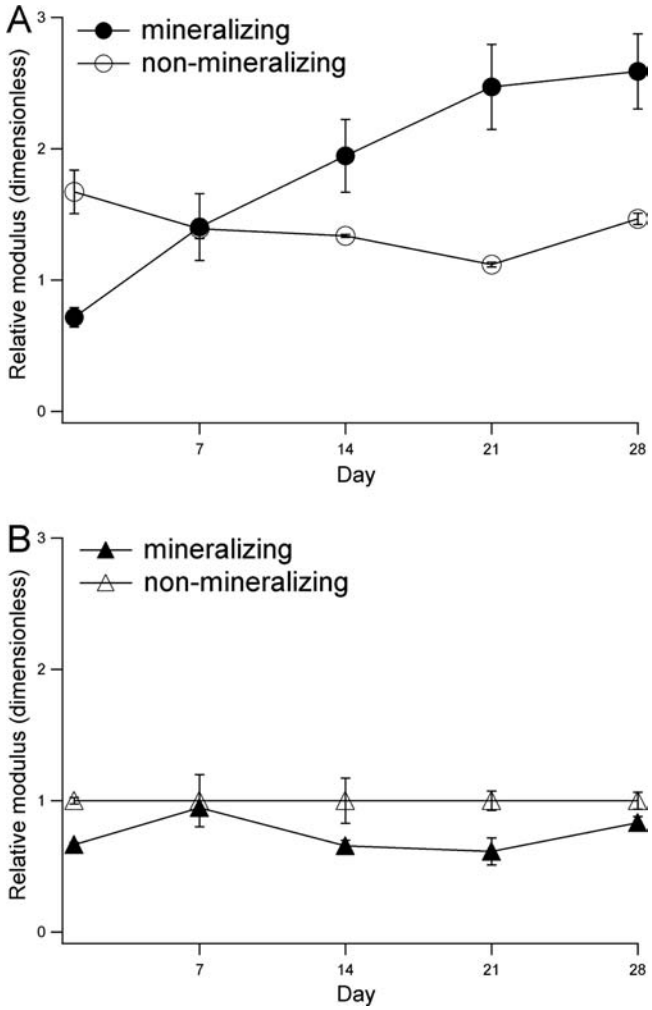

FIG. 4. Mean values (±SE) of the relative elastic modulus of MC3T3-E1 cells cultured on (**A**) SPS and (**B**) Si. Modulus values were normalized relative to the modulus of day 1 nonmineralizing cells on Si. The atomic force microscope was used in contact mode with a silicon nitride tip (spring constant 0.06 N/m). The x-direction piezo was oscillated at a sinusoidal frequency of 1400 Hz, and a constant normal force of 25 nN was applied to maintain contact between the tip and the cell surface.

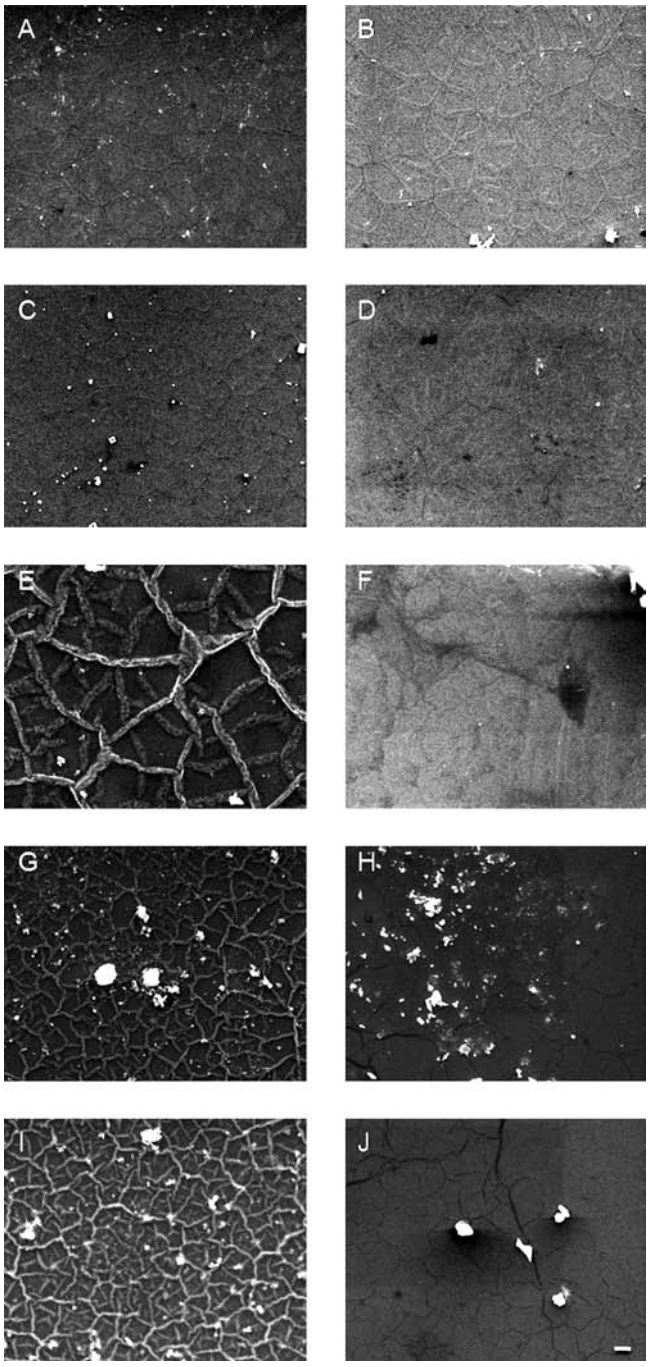

FIG. 5. Scanning electron micrographs of mineralizing (**A, C, E, G, I**) and nonmineralizing (**B, D, F, H, J**) MC3T3-E1 cultures on SPS after incubation in osteogenic medium for 1 (**A, B**), 7 (**C, D**), 14 (**E, F**), 21 (**G, H**), and 28 (**I, J**) days. Bar = 10 μm.

particles found in the 28-day mineralizing cultures was close to the synthetic HAP we tested against (Ca/P = 1.42), as well as to 30-day osteoblast cell culture as verified by atomic absorption spectroscopy in a similar study.[13] One caveat in interpreting EDS data is that these values may be considerably affected by scattering from proteins in the sample as well as the substrate, and therefore EDS is not a precise method and should only be considered in relative terms, as these ratios do not accurately represent the mineral quality or phase of the sample.[11]

Synchrotron GIXD data showed broad, prominent [002], and [211]/[112] peaks of HAP in the 14-, 21-, and 28-day mineralizing MC3T3-E1 cultures (Fig. 7A). These patterns average over an illuminated X-ray beam footprint 0.2- to 0.3-mm wide × 6- to 10-mm long. No peaks were seen in the 1- or 7-day mineralizing cultures (Fig. 7A), or any of the nonmineralizing cultures (Fig. 7B). Areas under the peaks were integrated to estimate the amount of HAP on the sample and were shown to increase for the mineralizing cells at day 14 and again at day 28 (Fig. 7C). A separate set of experiments was repeated and showed the same trend in mineral accumulation.

The sizes of the [002] HAP crystallites were calculated to be between 13 and 16 nm (Table 1), comparable to reported crystallite sizes in the literature.[13,35,36,42] It is interesting that

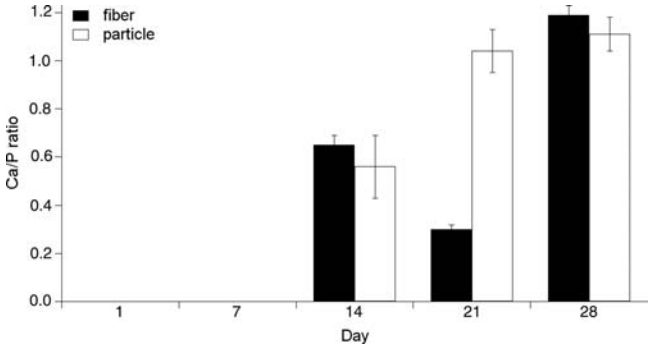

FIG. 6. Mean (±SE) Ca/P ratios calculated from EDS data on ECM fibers and particles from mineralizing samples seen in Figure 5. An average of three fibers and three particles is shown for each sample. The synthetic HAP standard had a Ca/P value of 1.42. Ca/P values from the nonmineralizing samples were zero at all time points.

the crystallites increased slightly in size from day 14 to day 21, and then decreased from day 21 to day 28. Because smaller crystallites may have an advantage in being resistant to dissolution and are therefore more stable,[43] this may explain why the day-28 crystals are smaller than those from day 21. The increase in crystallite size on day 21 also coincides with the abrupt increase in Ca/P ratio of the calcium particles (Fig. 6), indicating that by the third week there may have been a decrease in the phosphate concentration in the crystallites. Extracellular phosphate levels have been shown to upregulate the expression of osteopontin, a late differentiation marker that is strongly expressed in osteoblasts at day 21.[44] Our findings suggest that around day 21, phosphates in the ECM may have been increasingly utilized for the expression of osteopontin, making them less available for the formation of HAP crystallites and resulting in the higher Ca/P ratio.

Cell morphology

To further probe factors that contributed to the mechanical stiffness of the MC3T3-E1 cells, we chose actin restructuring as a visible, trackable phenotypic differentiation marker. F-actin was visualized in the green channel and nuclei were visualized in the red channel using immunofluorescence microscopy. The mineralizing subclone on SPS on days 1 (Fig. 8A) and 7 (Fig. 8B) initially possessed a fibroblastic morphology, with clearly visible, web-like actin filaments that are characteristic of differentiating osteoblasts.[45,46] On day 14 the actin structure in these cells seemed to have retracted to the cellular periphery in the shape of small bundles (Fig. 8C). These morphological changes are known to be a natural progression for osteogenic cells, indicating ECM protein production[47] and differentiation into osteoblasts.[46]

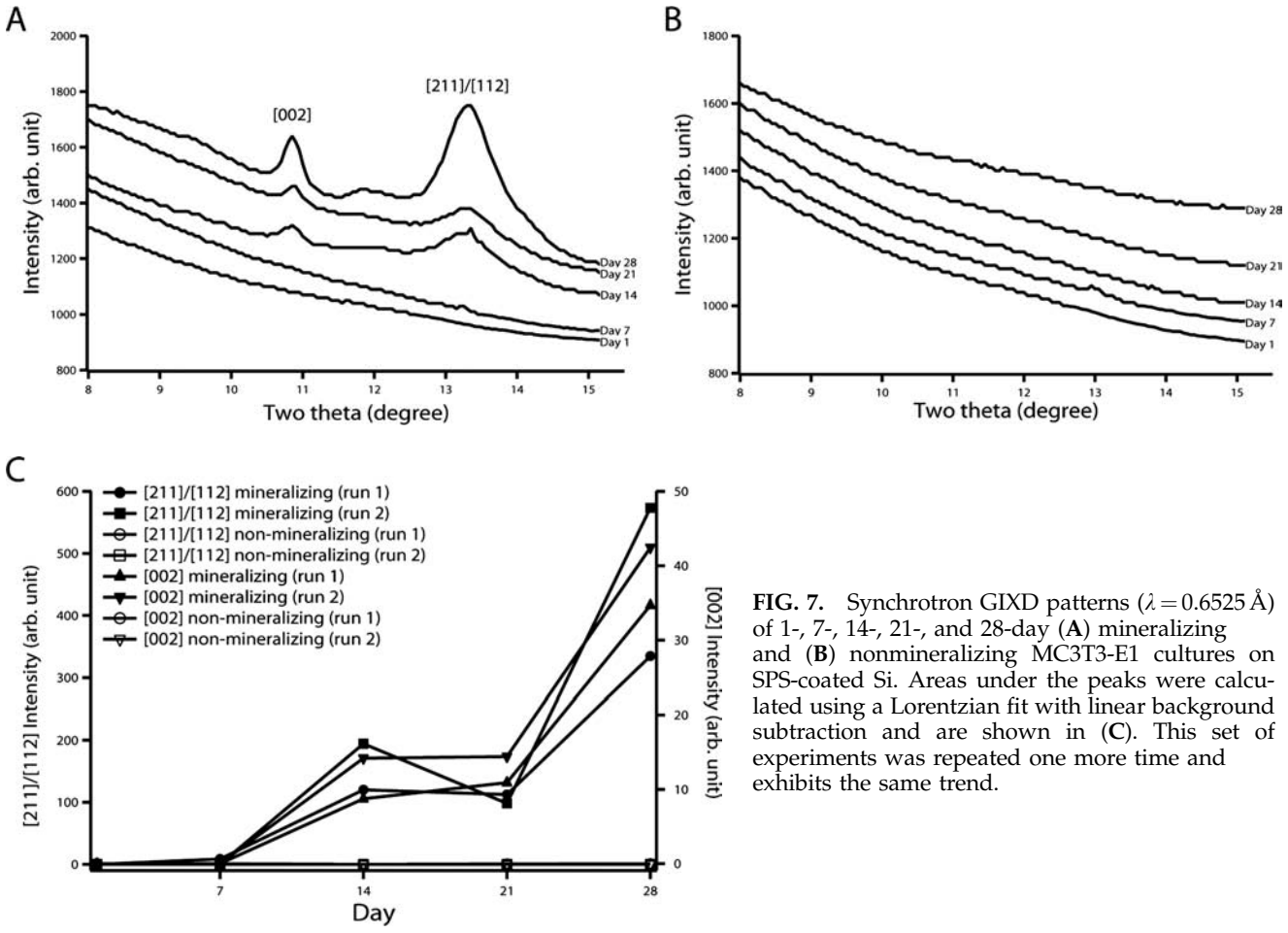

FIG. 7. Synchrotron GIXD patterns ($\lambda = 0.6525$ Å) of 1-, 7-, 14-, 21-, and 28-day (**A**) mineralizing and (**B**) nonmineralizing MC3T3-E1 cultures on SPS-coated Si. Areas under the peaks were calculated using a Lorentzian fit with linear background subtraction and are shown in (**C**). This set of experiments was repeated one more time and exhibits the same trend.

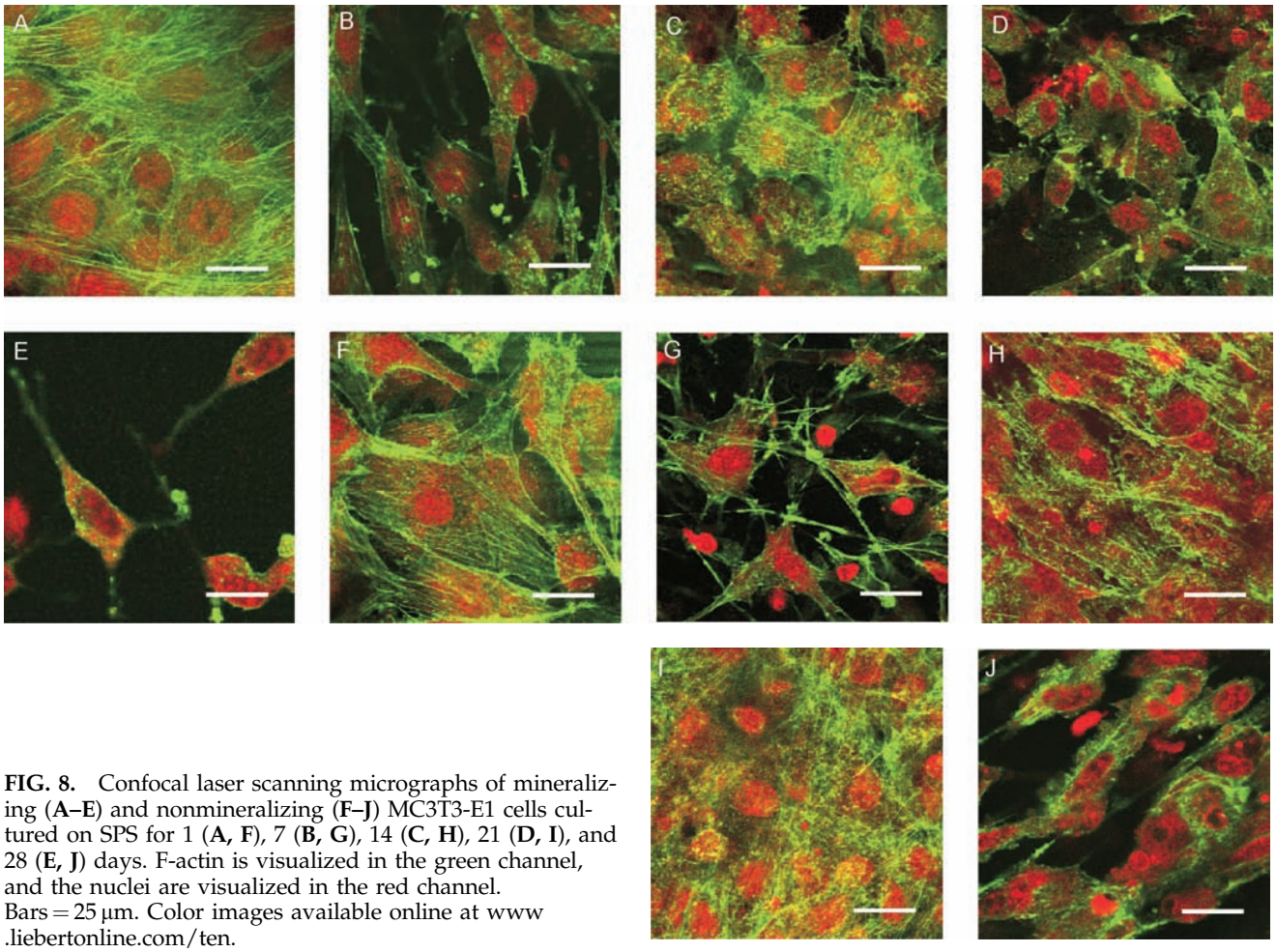

FIG. 8. Confocal laser scanning micrographs of mineralizing (**A–E**) and nonmineralizing (**F–J**) MC3T3-E1 cells cultured on SPS for 1 (**A, F**), 7 (**B, G**), 14 (**C, H**), 21 (**D, I**), and 28 (**E, J**) days. F-actin is visualized in the green channel, and the nuclei are visualized in the red channel. Bars = 25 μm. Color images available online at www.liebertonline.com/ten.

This retraction/reorganization of the actin filaments coincides with the first appearance of HAP peaks in our GIXD study (Fig. 7A). By day 21, the nuclei appeared much smaller (Fig. 8D), and by day 28, these appeared to have lost much of the actin structure (Fig. 8E).

The nonmineralizing cells on SPS initially were also fibroblastic in appearance (Fig. 8F). However, they did not show the cobblestone-like morphology beyond day 1. On day 7 these cells became more spindle like (Fig. 8G), with a reduced cytoskeletal network. On day 14, the nonmineralizing cells on SPS became very elongated and the individual cells appeared to align in a parallel fashion (Fig. 8H). By day 21, the nuclei appeared much smaller (Fig. 8I), and by day 28, the cytoskeletal organization of these cells remained unperturbed (Fig. 8J). An overall comparison of the mineralizing sequence (A–E) to the nonmineralizing (F–J) shows fewer interruptions in the intercellular actin network continuity for the nonmineralizing cells.

Table 1. Volume-Weighted Average Size (±SD) of [002] HAP Crystallites in Mineralizing MC3T3-E1 Cultures on SPS-Coated Si

Day	*Crystallite size (nm)*
14	13.6 ± 0.01
21	16.0 ± 0.02
28	12.7 ± 0.01

Crystallite size was calculated from the full-width-half-maximum of corresponding peaks in the GIXD data according to the Scherrer method. No HAP peaks were seen for 1-day-old and 7-day-old mineralizing or any of the nonmineralizing samples.

On Si, the mineralizing cells on day 1 (Fig. 9A) had a similar cytomorphology as the mineralizing cells on SPS (Fig. 8A) and were fibroblast like with a clearly defined actin structure. By day 7, however, these cells lost their cytoskeletal integrity, with very few actin fibers visible among clusters (Fig. 9B). On day 14, more of the intercellular cytoskeletal network was lost, and some of the nuclei began to appear deteriorated (Fig. 9C). By day 21, the nuclei of these mineralizing cells on Si were further reduced in size (Fig. 9D), and by day 28 these cells retained very little of their original cytoskeletal structure (Fig. 9E).

The nonmineralizing subclone on Si also exhibited a fibroblast-like cytomorphology on days 1 (Fig. 9F) and 7 (Fig. 9G). On days 14, 21, and 28, these cells did not appear to differ greatly in morphology from the previous time points and still possessed much of the actin at the end of the 4 weeks (Fig. 9H–J). When the nonmineralizing cells on SPS (Fig. 8F–J) and Si (Fig. 9F–J) are now compared, it is seen that their evolution is rather similar. These cells do not attempt significant reworking of the ECM. Instead, they produce a comparatively static actin network that is not greatly affected by the substrate. The situation for mineralizing cells is dra-

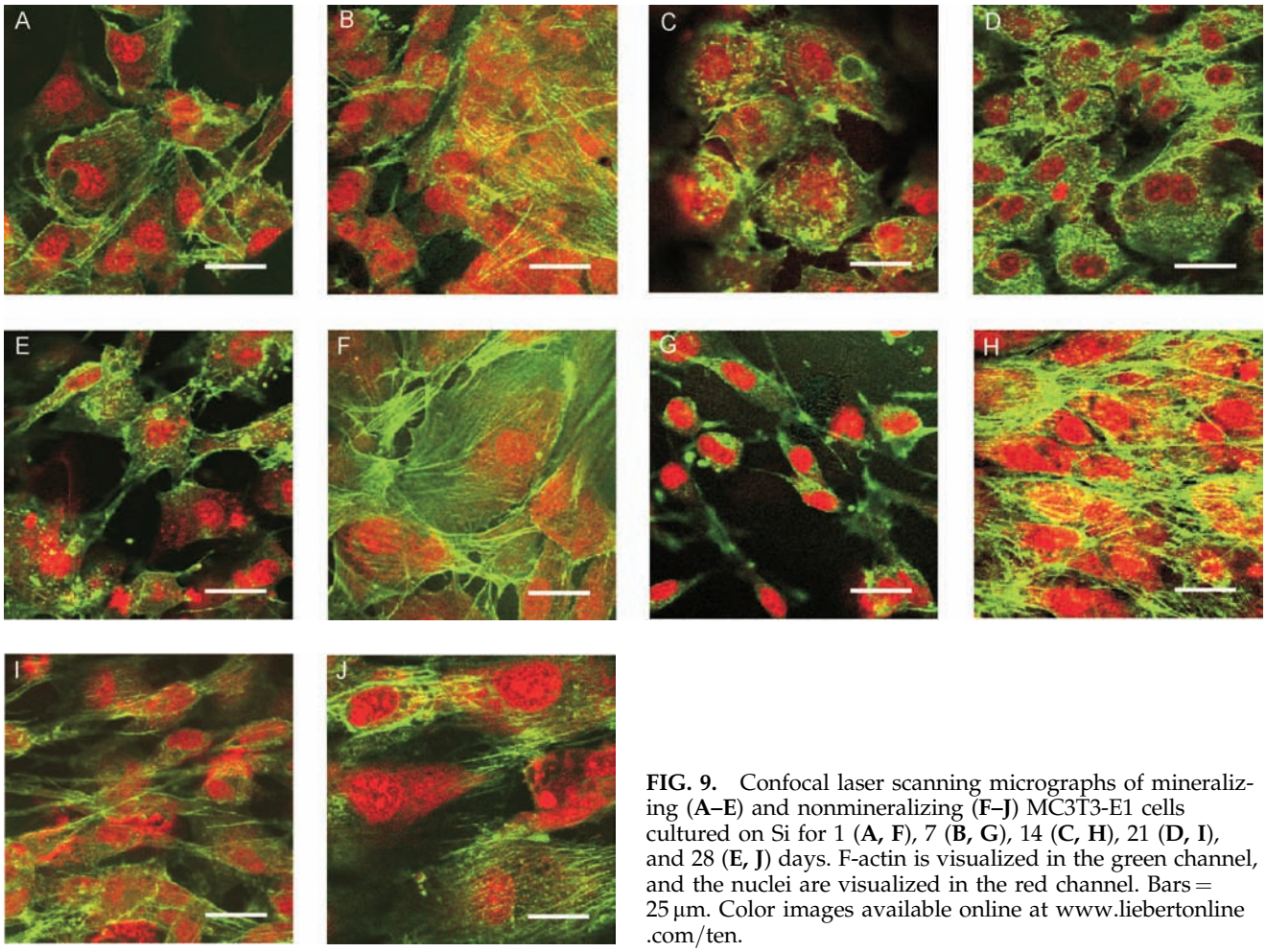

FIG. 9. Confocal laser scanning micrographs of mineralizing (**A–E**) and nonmineralizing (**F–J**) MC3T3-E1 cells cultured on Si for 1 (**A, F**), 7 (**B, G**), 14 (**C, H**), 21 (**D, I**), and 28 (**E, J**) days. F-actin is visualized in the green channel, and the nuclei are visualized in the red channel. Bars = 25 μm. Color images available online at www.liebertonline.com/ten.

matically different. On SPS they are seen to progress through several stages of ECM development, and this is supported by ECM and cell mechanics data discussed above. On Si, they are prevented from proper ECM formation. Cell culture integrity and the ability to mineralize suffer as a result.

An examination of the nuclear volume extracted from three-dimensional confocal laser scanning microscopy (CLSM) data reveals that mineralizing cells on SPS remained the most flattened throughout the 4 weeks (Fig. 10A). There was a fourfold increase on day 14, which may have resulted from actin restructuring as evident in their cuboidal morphology (Fig. 8C, D). This was followed by a gradual return to initial dimensions by day 28. The nonmineralizing cells on SPS initially were much larger in nuclear volume than their mineralizing counterparts and remained larger at the other time points, without exhibiting an overall trend in cell shape or volumetric change. On bare Si (Fig. 10B), mineralizing cells had much larger nuclei than when they were cultured on SPS at all time points, with a maximum seen on day 7 that coincided with the appearance of actin bundles (Fig. 9B), as these cells may have been attempting a restructuring of the actin cytoskeleton. However, by day 28, these actin bundles were no longer visible. The nonmineralizing cells on Si did not appear to undergo much change in nuclear dimensions and, except for day 7, were similar in size to their mineralizing counterparts on Si (Fig. 10B). There was a slight increase on day 28, corresponding to the loss of intact actin fibers (Fig. 9J).

These observations, together with the SEM and GIXD data, strongly suggest that proper differentiation and mineralization did not occur for nonmineralizing cells on SPS or for either subclone cultured on Si.

Discussion

Our experiments demonstrate that cell-mediated mineralization only occurred on a substrate that induced protein adsorption and network formation, which were needed for ECM development. Even though the nonmineralizing subclone produced an ECM, it was less stiff than that produced by the mineralizing subclone and was not mineralized during the 4 weeks. By monitoring the time dependence of ECM and cellular mechanical properties, we observed changes in the mineralizing subclone, evidently linked to ECM differentiation, which did not occur in nonmineralizing cells. These results signify that the mere presence of an ECM is not sufficient for the production of bone mineral, even though *in vitro* mineralization studies using supersaturated solutions can always be performed. In the nonmineralizing subclone, along with lack of proper ECM formation, the cells are probably lacking other crucial mineralization processes. The

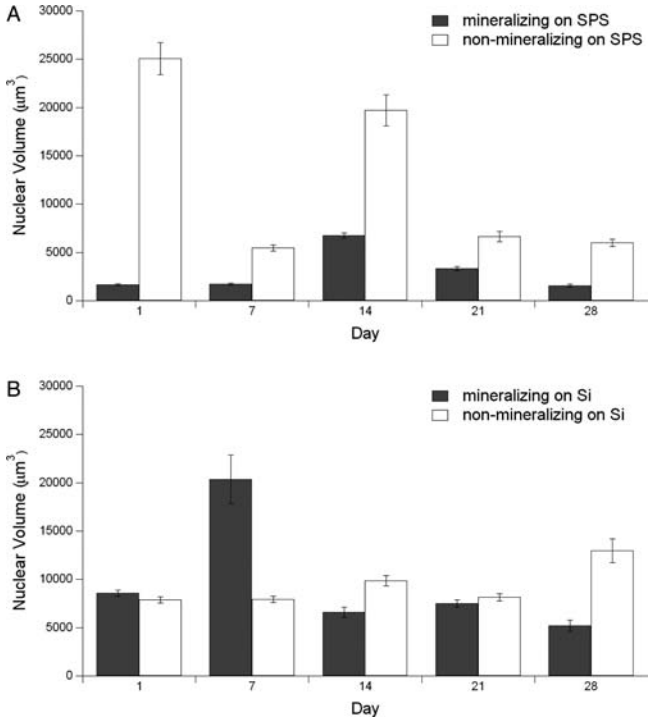

FIG. 10. Mean (±SE) volume of nuclei in mineralizing and nonmineralizing MC3T3-E1 cultures on SPS (**A**) and Si (**B**).

difference between the mineralizing and the nonmineralizing subclone is most evident in the presence and absence, respectively, of HAP nanocrystals in the sample after 28 days of incubation in osteogenic medium.

This is why our comparison of SPS to Si is so illuminating. On Si, the mineralizing cells adhere to the substrate for the duration of the study, but no ECM is formed and subsequently biomineralization is not observed. The properties of the ECM are of critical importance, and its development can evidently be prevented by both environmental and genetic factors.

The substrate also affects actin formation. The CLSM images shown in Figures 8 and 9 vividly demonstrate the difference between cells with intact actin fibers versus those that have reduced cytoskeletal integrity. However, even though actin stress fibers were visible in the nonmineralizing cells on SPS on day 28, their elastic modulus was not different from day 1, indicating that cell elasticity is not only due to an intact actin structure and that other factors need to be considered. The increase in the stiffness of mineralizing MC3T3-E1 cells on SPS suggests that cytoskeletal remodeling activity[48] may have led to the rearrangement of the F-actin network. The physical interrelationships between cultured (or implanted) biomineralizing cells, their ECM, and their substrate remain to be further elucidated.

A priority for our future research is to determine the components of the varying ECMs in our system and to relate this information to the prospects for seeding cells for regenerative tissue engineering. By understanding the mechanism of biomineralization in osteoblasts through their interactions with the ECM, we can eventually create an engineered bone tissue scaffold to accelerate bone formation and regeneration.

Summary

We examined the mechanical modulus, chemical properties, mineral production, and cytomorphology of mineralizing and nonmineralizing MC3T3-E1 osteoblast-like cells and their ECM fibers maintained in osteogenic medium for up to 4 weeks. Using SMFM, we found that the elastic modulus of living osteoblasts increased with time only for the mineralizing subclone on the SPS surface, with a concomitant increase in HAP production that was verified by synchrotron GIXD and EDS. Interestingly, the ECM fibers of the mineralizing subclone were much stiffer than their nonmineralizing counterparts on day 1, and grew thicker and wider with time for both subclones when cultured on SPS. After 1 week, the stiffness of the fibers became bimodal in the mineralizing culture, but remained unimodal in the nonmineralizing ECM. Ca/P ratios from EDS analysis showed that the fibers of the mineralizing subclone contained no calcium on days 1 and 7, and may have contained amorphous HAP on days 14 and 21. By day 28 these fibers had Ca/P ratios that approached those of crystalline HAP. The particles found in the mineralizing ECM on day 14 had a similar Ca/P as the fibers on the same day, but increased in calcium content by days 21 and 28. GIXD data showed that HAP found in the mineralizing subclone on days 14, 21, and 28 had an average [002] HAP crystallite size of 13.6, 16.0, and 12.7, respectively. CLSM revealed a restructuring of the actin cytoskeleton only for mineralizing osteoblasts cultured on SPS. Such evidence of remodeling activities was not seen in any of the other samples, and no ECM networks were observed for cells cultured on bare Si. These results show that the correct and complete development of the ECM network is required for osteoblasts to mineralize. This in turn requires a suitably prepared synthetic substrate for bone development to succeed *in vitro*.

Acknowledgments

The MC3T3-E1 cell lines were kindly donated by B. Frenkel and L. Bonewald. Many thanks to S. Ge and J. Sokolov for their assistance with the AFM and the CLSM. Thanks also to A. Stein and J. Warren for their help with the SEM. This work is kindly supported at Stony Brook University by the NIH (R01 AR49286, Y.Q. and R01 AR52379, Y.Q.), U.S. Army Medical Research and Materiel Command (DAMD-17-02-1-0218, Y.Q.), NSF, MRSEC, and DOE. Brookhaven National Laboratory is supported under U.S. DOE Contract DE-AC02-98CH10886.

References

1. Globus, R.K., Doty, S.B., Lull, J.C., Holmuhamedov, E., Humphries, M.J., and Damsky, C.H. Fibronectin is a survival factor for differentiated osteoblasts. J Cell Sci **111,** 1385, 1998.
2. Bissell, M.J., Hall, H.G., and Parry, G. How does the extracellular-matrix direct gene-expression. J Theor Biol **99,** 31, 1982.
3. Marsh, M.E., Munne, A.M., Vogel, J.J., Cui, Y.Q., and Franceschi, R.T. Mineralization of bone-like extracellular-matrix in the absence of functional osteoblasts. J Bone Miner Res **10,** 1635, 1995.
4. Chen, X.D., Dusevich, V., Feng, J.Q., Manolagas, S.C., and Jilka, R.L. Extracellular matrix made by bone marrow cells

facilitates expansion of marrow-derived mesenchymal progenitor cells and prevents their differentiation into osteoblasts. J Bone Miner Res **22,** 1943, 2007.
5. Shin, H., Jo, S., and Mikos, A.G. Biomimetic materials for tissue engineering. Biomaterials **24,** 4353, 2003.
6. Ge, S., Pu, Y., Zhang, W., Rafailovich, M., Sokolov, J., Buenviaje, C., Buckmaster, R., and Overney, R.M. Shear modulation force microscopy study of near surface glass transition temperatures. Phys Rev Lett **85,** 2340, 2000.
7. Subburaman, K., Pernodet, N., Kwak, S.Y., DiMasi, E., Ge, S., Zaitsev, V., Ba, X., Yang, N.L., and Rafailovich, M. Templated biomineralization on self-assembled protein fibers. Proc Natl Acad Sci USA **103,** 14672, 2006.
8. Chung, E.H., Gilbert, M., Virdi, A.S., Sena, K., Sumner, D.R., and Healy, K.E. Biomimetic artificial ECMs stimulate bone regeneration. J Biomed Mater Res A **79A,** 815, 2006.
9. Tampieri, A., Sandri, M., Landi, E., Celotti, G., Roveri, N., Mattioli-Belmonte, M., Virgili, L., Gabbanelli, F., and Biagini, G. HA/alginate hybrid composites prepared through bioinspired nucleation. Acta Biomater **1,** 343, 2005.
10. Kretlow, J.D., and Mikos, A.G. Review: Mineralization of synthetic polymer scaffolds for bone tissue engineering. Tissue Eng **13,** 927, 2007.
11. Boskey, A. Bone mineralization. In: Cowin, S.C., ed. Bone Mechanics Handbook. Boca Raton: CRC Press, 2001.
12. Bonewald, L.F., Harris, S.E., Rosser, J., Dallas, M.R., Dallas, S.L., Camacho, N.P., Boyan, B., and Boskey, A. Von Kossa staining alone is not sufficient to confirm that mineralization *in vitro* represents bone formation. Calcif Tissue Int **72,** 537, 2003.
13. Rey, C., Kim, H.M., Gerstenfeld, L., and Glimcher, M.J. Structural and chemical characteristics and maturation of the calcium-phosphate crystals formed during the calcification of the organic matrix synthesized by chicken osteoblasts in cell-culture. J Bone Miner Res **10,** 1577, 1995.
14. Stewart, S., Shea, D.A., Tarnowski, C.P., Morris, M.D., Wang, D., Franceschi, R., Lin, D.L., and Keller, E. Trends in early mineralization of murine calvarial osteoblastic cultures: a Raman microscopic study. J Raman Spectrosc **33,** 536, 2002.
15. Kuhn, L.T., Xu, Y.T., Rey, C., Gerstenfeld, L.C., Grynpas, M.D., Ackerman, J.L., Kim, H.M., and Glimcher, M.J. Structure, composition, and maturation of newly deposited calcium-phosphate crystals in chicken osteoblast cell cultures. J Bone Miner Res **15,** 1301, 2000.
16. Hartgerink, J.D., Beniash, E., and Stupp, S.I. Self-assembly and mineralization of peptide-amphiphile nanofibers. Science **294,** 1684, 2001.
17. Landi, E., Tampieri, A., Celotti, G., Langenati, R., Sandri, M., and Sprio, S. Nucleation of biomimetic apatite in synthetic body fluids: dense and porous scaffold development. Biomaterials **26,** 2835, 2005.
18. Leventouri, T. Synthetic and biological hydroxyapatites: crystal structure questions. Biomaterials **27,** 3339, 2006.
19. Declercq, H.A., Verbeeck, R.M.H., de Ridder, L., Schacht, E.H., and Cornelissen, M.J. Calcification as an indicator of osteoinductive capacity of biomaterials in osteoblastic cell cultures. Biomaterials **26,** 4964, 2005.
20. Hollinger, J.O., Brekke, J., Gruskin, E., and Lee, D. Role of bone substitutes. Clin Orthop Rel Res **324,** 55, 1996.
21. Green, D., Walsh, D., Mann, S., and Oreffo, R.O.C. The potential of biomimesis in bone tissue engineering: lessons from the design and synthesis of invertebrate skeletons. Bone **30,** 810, 2002.
22. Sharma, B., and Elisseeff, J.H. Engineering structurally organized cartilage and bone tissues. Ann Biomed Eng **32,** 148, 2004.
23. Liu, X.H., and Ma, P.X. Polymeric scaffolds for bone tissue engineering. Ann Biomed Eng **32,** 477, 2004.
24. Ishaug-Riley, S.L., Crane, G.M., Gurlek, A., Miller, M.J., Yasko, A.W., Yaszemski, M.J., and Mikos, A.G. Ectopic bone formation by marrow stromal osteoblast transplantation using poly(DL-lactic-co-glycolic acid) foams implanted into the rat mesentery. J Biomed Mater Res **36,** 1, 1997.
25. Oest, M.E., Dupont, K.M., Kong, H.J., Mooney, D.J., and Guldberg, R.E. Quantitative assessment of scaffold and growth factor-mediated repair of critically sized bone defects. J Orthop Res **25,** 941, 2007.
26. Moursi, A.M., Damsky, C.H., Lull, J., Zimmerman, D., Doty, S.B., Aota, S.I., and Globus, R.K. Fibronectin regulates calvarial osteoblast differentiation. J Cell Sci **109,** 1369, 1996.
27. Cowles, E.A., Brailey, L.L., and Gronowicz, G.A. Integrin-mediated signaling regulates AP-1 transcription factors and proliferation in osteoblasts. J Biomed Mater Res **52,** 725, 2000.
28. Carvalho, R.S., Kostenuik, P.J., Salih, E., Bumann, A., and Gerstenfeld, L.C. Selective adhesion of osteoblastic cells to different integrin ligands induces osteopontin gene expression. Matrix Biol **22,** 241, 2003.
29. van den Dolder, J., Bancroft, G.N., Sikavitsas, V.I., Spauwen, P.H.M., Mikos, A.G., and Jansen, J.A. Effect of fibronectin- and collagen I-coated titanium fiber mesh on proliferation and differentiation of osteogenic cells. Tissue Eng **9,** 505, 2003.
30. Garcia, A.J., Takagi, J., and Boettiger, D. Two-stage activation for alpha(5)beta(1) integrin binding to surface-adsorbed fibronectin. J Biol Chem **273,** 34710, 1998.
31. Liu, Y., Yanai, R., Lu, Y., Kimura, K., and Nishida, T. Promotion by fibronectin of collagen gel contraction mediated by human corneal fibroblasts. Exp Eye Res **83,** 1196, 2006.
32. Greiling, D., and Clark, R.A.F. Fibronectin provides a conduit for fibroblast transmigration from collagenous stroma into fibrin clot provisional matrix. J Cell Sci **110,** 861, 1997.
33. Pernodet, N., Rafailovich, M., Sokolov, J., Xu, D., Yang, N.L., and McLeod, K. Fibronectin fibrillogenesis on sulfonated polystyrene surfaces. J Biomed Mater Res A **64A,** 684, 2003.
34. Sudo, H., Kodama, H.A., Amagai, Y., Yamamoto, S., and Kasai, S. *In vitro* differentiation and calcification in a new clonal osteogenic cell-line derived from newborn mouse calvaria. J Cell Biol **96,** 191, 1983.
35. Danilchenko, S.N., Kukharenko, O.G., Moseke, C., Protsenko, I.Y., Sukhodub, L.F., and Sulkio-Cleff, B. Determination of the bone mineral crystallite size and lattice strain from diffraction line broadening. Cryst Res Technol **37,** 1234, 2002.
36. Rusu, V.M., Ng, C.H., Wilke, M., Tiersch, B., Fratzl, P., and Peter, M.G. Size-controlled hydroxyapatite nanoparticles as self-organized organic-in organic composite materials. Biomaterials **26,** 5414, 2005.
37. Franceschi, R.T., and Iyer, B.S. Relationship between collagen-synthesis and expression of the osteoblast phenotype in Mc3t3-E1 cells. J Bone Miner Res **7,** 235, 1992.
38. Wang, D., Christensen, K., Chawla, K., Xiao, G.Z., Krebsbach, P.H., and Franceschi, R.T. Isolation and characterization of MC3T3-E1 preosteoblast subclones with distinct *in vitro* and *in vivo* differentiation mineralization potential. J Bone Miner Res **14,** 893, 1999.

39. Lo, C.M., Wang, H.B., Dembo, M., and Wang, Y.L. Cell movement is guided by the rigidity of the substrate. Biophys J **79,** 144, 2000.
40. Engler, A., Bacakova, L., Newman, C., Hategan, A., Griffin, M., and Discher, D. Substrate compliance versus ligand density in cell on gel responses. Biophys J **86,** 617, 2004.
41. Engler, A.J., Griffin, M.A., Sen, S., Bonnetnann, C.G., Sweeney, H.L., and Discher, D.E. Myotubes differentiate optimally on substrates with tissue-like stiffness: pathological implications for soft or stiff microenvironments. J Cell Biol **166,** 877, 2004.
42. Hu, Q.H., Tan, Z., Liu, Y.K., Tao, J.H., Cai, Y.R., Zhang, M., Pan, H.H., Xu, X.R., and Tang, R.K. Effect of crystallinity of calcium phosphate nanoparticles on adhesion, proliferation, and differentiation of bone marrow mesenchymal stem cells. J Mater Chem **17,** 4690, 2007.
43. Tang, R.K., Wang, L.J., Orme, C.A., Bonstein, T., Bush, P.J., and Nancollas, G.H. Dissolution at the nanoscale: self-preservation of biominerals. Angew Chem Int Ed **43,** 2697, 2004.
44. Beck, G.R., Zerler, B., and Moran, E. Phosphate is a specific signal for induction of osteopontin gene expression. Proc Natl Acad Sci USA **97,** 8352, 2000.
45. Domke, J., Dannohl, S., Parak, W.J., Muller, O., Aicher, W.K., and Radmacher, M. Substrate dependent differences in morphology and elasticity of living osteoblasts investigated by atomic force microscopy. Colloids Surf B Biointerfaces **19,** 367, 2000.
46. Rodriguez, J.P., Gonzalez, M., Rios, S., and Cambiazo, V. Cytoskeletal organization of human mesenchymal stem cells (MSC) changes during their osteogenic differentiation. J Cell Biochem **93,** 721, 2004.
47. Krause, A., Cowles, E.A., and Gronowicz, G. Integrin-mediated signaling in osteoblasts on titanium implant materials. J Biomed Mater Res **52,** 738, 2000.
48. Takai, E., Costa, K.D., Shaheen, A., Hung, C.T., and Guo, X.E. Osteoblast elastic modulus measured by atomic force microscopy is substrate dependent. Ann Biomed Eng **33,** 963, 2005.
49. DiMasi, E., *et al.* Biomimetic and bioinspired chemistry. In: Behrens, P., and Bäueralein, E., eds. Handbook of Biomineralization. Weinherm, Germany: Wiley-VCH, 2007, pp. 119–133.

Address reprint requests to:
Yi-Xian Qin, Ph.D.
Department of Biomedical Engineering
Stony Brook University
Psychology-A Building, 3rd Floor
Stony Brook, NY 11794-2580

E-mail: yi-xian.qin@sunysb.edu

Received: November 6, 2007
Accepted: May 19, 2008
Online Publication Date: August 29, 2008